Article

Developmental Cell

Fibroblast dedifferentiation as a determinant of successful regeneration

Graphical abstract

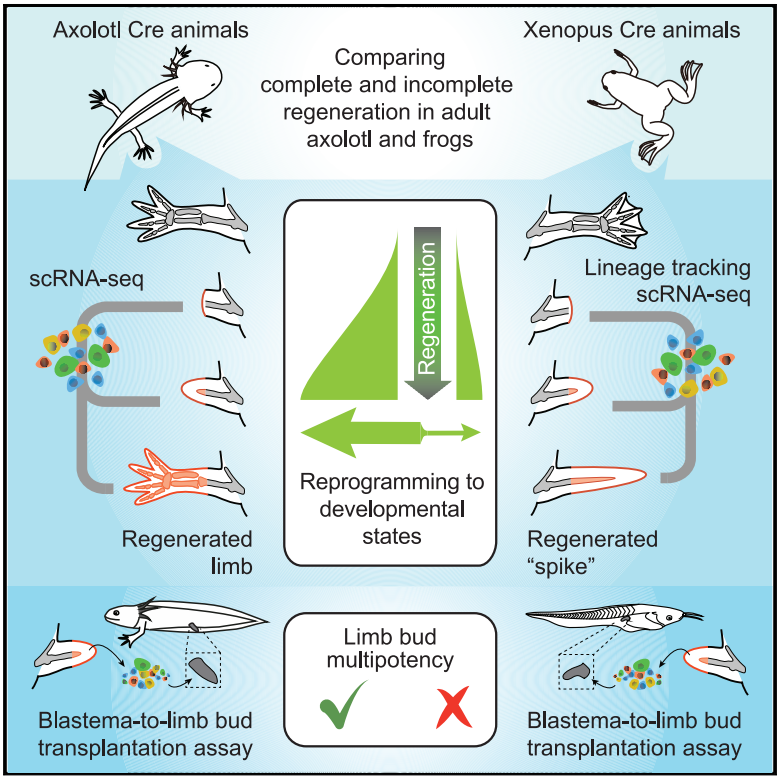

Highlights

- Fibroblast-derived Prrx1^{+} cells are the main constituent of a frog limb blastema
- Frog fibroblasts only undergo partial dedifferentiation due to intrinsic limitations
- Adult chondrogenesis is distinct from the embryonic program

Authors

Tzi-Yang Lin, Tobias Gerber, Yuka Taniguchi-Sugiura, ..., Eri Shibata, Barbara Treutlein, Elly M. Tanaka

Correspondence

barbara.treutlein@bsse.ethz.ch (B.T.), elly.tanaka@imp.ac.at (E.M.T.)

In brief

Lin et al. systematically compared the response to limb amputation in axolotls and African clawed frogs. Unlike in axolotls, frog limb fibroblasts are incapable of fully re-activating developmental programs required for complete limb regeneration. This work defines intrinsic restrictions in fibroblasts as a limitation to adult regeneration.

Lin et al., 2021, Developmental Cell *56*, 1541–1551
May 17, 2021
https://doi.org/10.1016/j.devcel.2021.04.016

CellPress

Developmental Cell

CellPress
OPEN ACCESS

Article

Fibroblast dedifferentiation as a determinant of successful regeneration

Tzi-Yang Lin,[1,6] Tobias Gerber,[2,6,7] Yuka Taniguchi-Sugiura,[1,6] Prayag Murawala,[1,8] Sarah Hermann,[3] Lidia Grosser,[1] Eri Shibata,[5] Barbara Treutlein,[4,*] and Elly M. Tanaka[1,9,*]

[1]Research Institute of Molecular Pathology (IMP), Vienna BioCenter (VBC), 1030 Vienna, Austria
[2]Max Planck Institute for Evolutionary Anthropology, 04103 Leipzig, Germany
[3]DFG Research Center for Regenerative Therapies, Technische Universität Dresden, 01307 Dresden, Germany
[4]Department of Biosystems Science and Engineering, ETH Zürich, 4058 Basel, Switzerland
[5]School of Life Science and Technology, Tokyo Institute of Technology, 4259 Nagatsuta, Midori-ku, Yokohama 226-8501, Japan
[6]These authors contributed equally
[7]Present address: European Molecular Biology Laboratory (EMBL), 69117 Heidelberg, Germany
[8]Present address: Mount Desert Island Biological Laboratory, PO Box 35, Salisbury Cove, ME 04609, USA
[9]Lead contact
*Correspondence: barbara.treutlein@bsse.ethz.ch (B.T.), elly.tanaka@imp.ac.at (E.M.T.)
https://doi.org/10.1016/j.devcel.2021.04.016

SUMMARY

Limb regeneration, while observed lifelong in salamanders, is restricted in post-metamorphic *Xenopus laevis* frogs. Whether this loss is due to systemic factors or an intrinsic incapability of cells to form competent stem cells has been unclear. Here, we use genetic fate mapping to establish that connective tissue (CT) cells form the post-metamorphic frog blastema, as in the case of axolotls. Using heterochronic transplantation into the limb bud and single-cell transcriptomic profiling, we show that axolotl CT cells dedifferentiate and integrate to form lineages, including cartilage. In contrast, frog blastema CT cells do not fully re-express the limb bud progenitor program, even when transplanted into the limb bud. Correspondingly, transplanted cells contribute to extraskeletal CT, but not to the developing cartilage. Furthermore, using single-cell RNA-seq analysis we find that embryonic and adult frog cartilage differentiation programs are molecularly distinct. This work defines intrinsic restrictions in CT dedifferentiation as a limitation in adult regeneration.

INTRODUCTION

Limb regeneration capability varies among tetrapods, and the underlying causes for this diversity are unclear. Among amphibians, salamanders such as the axolotl (*Ambystoma mexicanum*) regenerate limbs as sexually mature adults, whereas frogs such as *Xenopus laevis*, studied here, lose regeneration capability during metamorphosis (Simon and Tanaka, 2013). In axolotls, limb amputation triggers the formation of a blastema, an accumulation of mesenchymal progenitors covered by an epithelium that rebuilds the missing limb, including fully patterned skeletal elements. Interestingly, the amputation of a post-metamorphic frog (stage 66) limb yields a proliferative response and the formation of a blastema that abortively forms a spike of unsegmented cartilage (Simon and Tanaka, 2013) (Figure 1A). Correspondingly, at the blastema stage, collagen and limb development factors are present in frog but show some divergent patterns to the axolotl blastema (Ohgo et al., 2010). Here, an important question is whether this abortive phenotype is mainly due to a deficient adult environment or an intrinsic incapability of blastema cells themselves (Sessions and Bryant, 1988). Multiple studies have attempted to enhance frog regeneration by supplementing the adult environment with additional cell types or extracellular factors (Herrera-Rincon et al., 2018; Lin et al., 2013; Mitogawa et al., 2018; Satoh et al., 2005; Yakushiji et al., 2009; Zhang et al., 2018). Other studies have stressed the potential negative impact of developing cartilage (Aztekin et al., 2020) or an adult immune system (Harty et al., 2003; King et al., 2012; Mescher et al., 2013). Correlative evidence shows a higher methylation state of a *shh* gene enhancer in adult frog cells compared with embryonic cells (Yakushiji et al., 2007). However, it has been challenging to disentangle the complex cohort of cells, tissues, and systemic environment to ascertain the defined limitations to regeneration.

One hindrance has been a lack of clarity of whether the same cell types build the axolotl and frog blastema and execute regeneration. During axolotl limb regeneration, descendants of the lateral plate mesoderm, collectively called as the connective tissue (CT), are major contributors to the early- and mid-bud limb blastema (Gerber et al., 2018; Kragl et al., 2009; Muneoka et al., 1986). The mature limb CT consists of multiple subtypes including dermal fibroblasts, interstitial fibroblasts, cartilage, bone, periosteum/perichondrium, ligaments, and tendons (Gerber et al., 2018; McCusker et al., 2015). Recently, genetic fate mapping combined with single-cell RNA sequencing (scRNA-seq) of CT cells in axolotls showed that dermal and interstitial CT fibroblasts are the major contributors to the blastema (Gerber et al., 2018). These fibroblasts dedifferentiate toward common, multipotent CT progenitors that rebuild the patterned

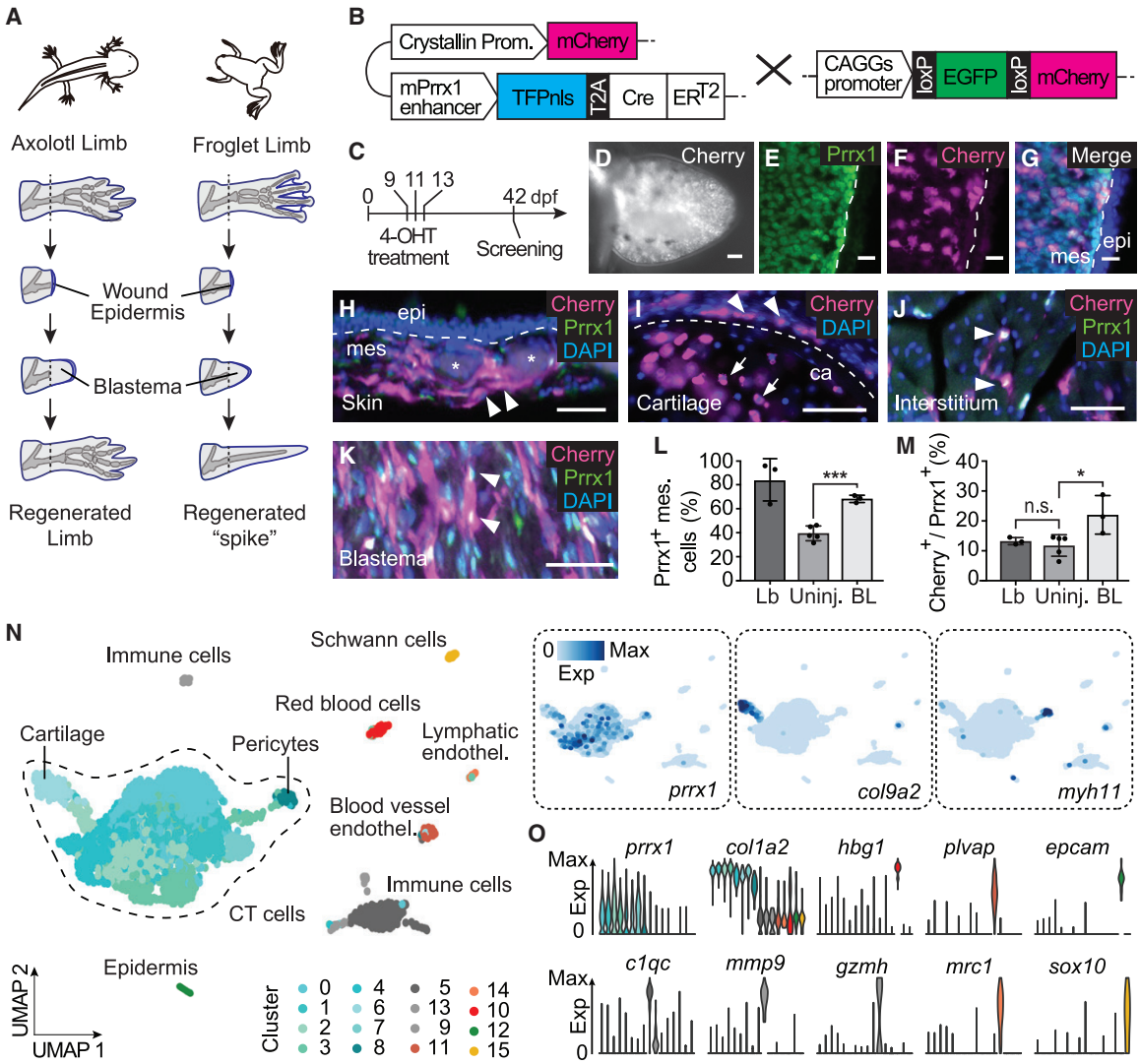

Figure 1. Connective tissue cells are source cells of the adult frog blastema

(A) Schematic comparison of limb regeneration after amputation in axolotls versus post-metamorphic frogs. Axolotls regenerate a complete limb while post-metamorphic frogs form a blastema but generate an abortive cartilage spike.

(B) Schematic illustration of the *Prrx1:CreER* line (left) and the *CAGGs:lp-Cherry* reporter line (right). The CreER cassette was codon optimized and each genotype was generated individually with the REMI protocol (see STAR methods for details). Germline transmitted *Prrx1:CreER* founders were mated with a *CAGGs:lp-Cherry* reporter line. The F1 carrying both *CreER* and reporter cassettes were screened and used for the experiments in this study.

(C) 4-hydroxytamoxifen (4-OHT) treatment paradigm used to convert the reporter cassette in F1.

(D) Whole-mount image of mCherry fluorescence of a hindlimb bud from a converted *Prrx1:CreER;CAGGs:lp-Cherry* transgenic stage 51 tadpole. Proximal: left; Distal: right. Scale bar represents 20 μm.

(E–G) Magnified fluorescence images of a longitudinal section of (D) immunostained for Prrx1 (mesenchymal CT cells, green) (E), Cherry (converted cells, magenta) (F), and the merged image with DAPI (nuclei, blue) (G). White dashed line denotes the border between Prrx1-positive mesenchyme (mes) and Prrx1-negative epidermis (epi). mCherry-expressing cells are confined to mesenchyme. Scale bars represent 20 μm.

(H) Transverse section of uninjured upper hindlimb skin from a converted *Prrx1:CreER;CAGGs:lp-Cherry* transgenic froglet, immunostained for Cherry (converted cells, magenta), Prrx1 (dermal CT cells, green), and DAPI (nuclei, blue). White arrowheads indicate examples of converted dermal fibroblasts identified as Cherry- and Prrx1-double positive cells at the mesenchyme (mes)-epidermis (epi) border (white dashed line). Asterisks indicate non-specific tissue autofluorescence. Scale bars represent 50 μm.

(I) Transverse section of cartilage region from a converted *Prrx1:CreER;CAGGs:lp-Cherry* transgenic froglet, immunostained for Cherry (converted cells, magenta) and DAPI (nuclei, blue). White dashed line denotes the border of cartilage (ca). White arrows indicate examples of converted Cherry-positive chondrocytes and white arrowheads the converted perichondria. Scale bars represent 50 μm.

(J) Transverse section of muscle bundle region from a converted *Prrx1:CreER;CAGGs:lp-Cherry* transgenic froglet, immunostained for Cherry (converted cells, magenta), Prrx1 (interstitial CT cells, green), and DAPI (nuclei, blue). White arrowheads indicate examples of converted interstitial fibroblasts identified as Cherry- and Prrx1-double positive cells. Scale bars represent 50 μm.

(legend continued on next page)

skeleton and CT. Such dedifferentiated blastema cells regain an embryonic gene expression program comparable to limb bud cells, including the patterning gene network. Here, we address the question whether frog CT fibroblasts make comparable contributions to the frog blastema and spike, and whether they dedifferentiate to fully potent limb bud progenitors. We reveal that the incapability of frog blastema cells to dedifferentiate back to limb-bud-like states is a key difference compared with axolotl blastema cells.

RESULTS

CT cells are source cells of the adult frog blastema

To determine if frog blastema cells have a comparable origin to axolotl blastema cells, we generated germline transgenic frog lines that express the tamoxifen-inducible Cre-ERT2 cassette under the control of the mouse *Prrx1* enhancer element (*Crystallin:mCherry;mPrrx1:xen(TFPnls-T2A-Cre-ERT2);CAGGs:lp-GFP-3pA-lp-mCherry-pA*, hereafter referred to as *Prrx1:CreER;CAGGs:lp-Cherry* animals) (Figures 1B and 1C) and performed genetic fate mapping. *Prrx1* has been established as a marker of CT precursors in the limb bud, and our previous work showed that CT-specific labeling could be achieved in axolotls using a mouse *Prrx1*-enhancer-driven Cre-ERT2 system with the administration of tamoxifen at limb bud stages (Gerber et al., 2018). Immunostaining with anti-PRRX1 antibody showed that Prrx1 is expressed in the majority of mesenchymal cells in developing stage 51 frog limb buds, as in the case of axolotls (Figures 1D, 1E, and 1L).

To track the contribution of CT cells to the blastema, we first induced recombination by tamoxifen administration at early embryonic stages (Figure 1C). 13.2% ± 1.2% of the limb bud Prrx1-positive cells underwent genomic recombination to express mCherry (Figures 1D–1G and 1M). The converted cells remained labeled after metamorphosis and were found in dermal, interstitial, perichondrial, and cartilage regions (Figures 1H–1J). Analysis of limb sections immunostained to detect Prrx1 protein showed that 11.7% ± 3.6% of Prrx1 protein-expressing cells expressed the Cherry transgene (Figure 1M), consistent with the embryonic conversion efficiency. We followed these converted cells during regeneration, where, after post-metamorphic limb amputation, mCherry-positive cells constituted 22.0% ± 6.5% of the Prrx1-expressing blastema cells that made up to 68.2% ± 3% of the blastema (Figures 1K–1M). This 2-fold enrichment of Cherry-positive cells indicated that the labeled *Prrx1*-descendant cells are potent contributors to the blastema. To further characterize the composition of the frog blastema, we performed scRNA-seq of cells dissociated from a frog blastema 14 days post-amputation (dpa) and visualized the data in two dimensions using uniform manifold approximation and projection (UMAP) embedding (Figures 1N and 1O). Clustering and marker gene expression analysis revealed that 85.3% of the dissociated cells showed CT signatures with 84.6% of CT cells expressing *prrx1* (Figures 1N and 1O). These blastema CT cells could be subcategorized into eight discernable subpopulations, including cartilage spike cells expressing *col9a2*, pericytes expressing *myh11*, and other blastema subpopulations. The remaining non-CT cell clusters included immune, endothelial, epidermal, and Schwann cells. Given that tissue dissociation can lead to distortions of cell type proportions, these observations concur satisfactorily with the 68.2% ± 3% of frog blastema mesenchyme cells observed to express Prrx1 protein (Figure 1L).

In axolotls, the *Prrx1*-descendants from the interstitium and dermis enter the blastema and converge to a common multipotent progenitor type that can regenerate all CT subtypes including skeleton, tendons, ligaments, interstitium, and dermis (Gerber et al., 2018). To ask whether frog CT subpopulations follow a similar program, we performed scRNA-seq analysis on blastema CT cells in a time course of limb regeneration spanning 0, 3, 7, 10, 14, 20, and 52 dpa (Figures 2A, 2B, S1A, and S1B), encompassing key time points of blastema establishment. Since our tracing results showed that *Prrx1*-converted Cherry-positive cells contribute potently to the blastema, and due to a lack of obvious blastema structure at 0 and 3 dpa, we FAC-sorted *Prrx1*-converted mCherry-positive cells from these time points from our *Prrx1:CreER;CAGGs:lp-Cherry* transgenic frogs for scRNA-seq. Importantly, the sorted cells clustered together with CT cells from an unsorted sample and we observed all representative CT subtypes in the sorted fraction (Figure S1C). The 0 and 3 dpa datasets were then combined with the extracted CT cell clusters of 7, 10, 14, 20, and 52 dpa datasets collected from whole blastemas (Figure S1A) (see STAR methods for details). We used Harmony (Korsunsky et al., 2019), a tool designed to integrate single-cell transcriptomic data across experiments and batches, to integrate the data across the different time points and UMAP to visualize the data in two dimensions. Clustering and marker gene expression analysis revealed four major mature CT subpopulations (excluding pericytes) in the intact tissue: interstitial cells (86.4%), dermal cells (4.9%), tenocytes (4.1%), and skeletal cells (3.6%) (Figure 2C; Table S1). The regeneration time course revealed a gradient of regenerating cell states across all blastema time points emerging from the

(K) Magnified fluorescence image of a longitudinal section of a 28 dpa blastema from a converted *Prrx1:CreER;CAGGs:lp-Cherry* transgenic froglet, immunostained for Cherry (converted cells, magenta), Prrx1 (blastema CT cells, green), and DAPI (nuclei, blue). Arrowheads show examples of the *Prrx1*-converted Cherry-positive cells contributing to the blastema. Scale bars represent 50 μm.

(L) Percentage of Prrx1-expressing mesenchymal cells in limb buds (Lb, 84.4% ± 17.7%, n = 3), uninjured leg (Uninj, 39.9% ± 5.6%, n = 5), and blastema (BL, 68.2% ± 3.0%, n = 3), determined by immunohistochemistry. Statistical significance is calculated using unpaired Student's t test. ***$p < 0.001$. Data are represented as mean ± SD.

(M) Percentage of converted Cherry+ CT precursors (Cherry+/Prrx1+) in limb buds (Lb, 13.2% ± 1.2%, n = 3), uninjured leg (Uninj, 11.7% ± 3.6%, n = 5), and blastema (BL, 22.0% ± 6.5%, n = 3), determined by immunohistochemistry. Statistical significance is calculated using unpaired Student's t test. n.s.: $p > 0.05$; *$p < 0.01$. Data are represented as mean ± SD.

(N) Uniform manifold approximation and projection (UMAP) embedding of scRNA-seq data of 3,817 cells from a 14-dpa frog blastema. Cells are colored by cluster and cell type annotations are noted. Insets show the expression of blastema cells with a CT signature (*prrx1*), pericyte (*myh11*), and cartilage (*col9a2*) markers projected onto the UMAP embedding.

(O) Violin plots show the expression of canonical marker genes defining cluster cell type annotations in the 14 dpa blastema as shown in (N).

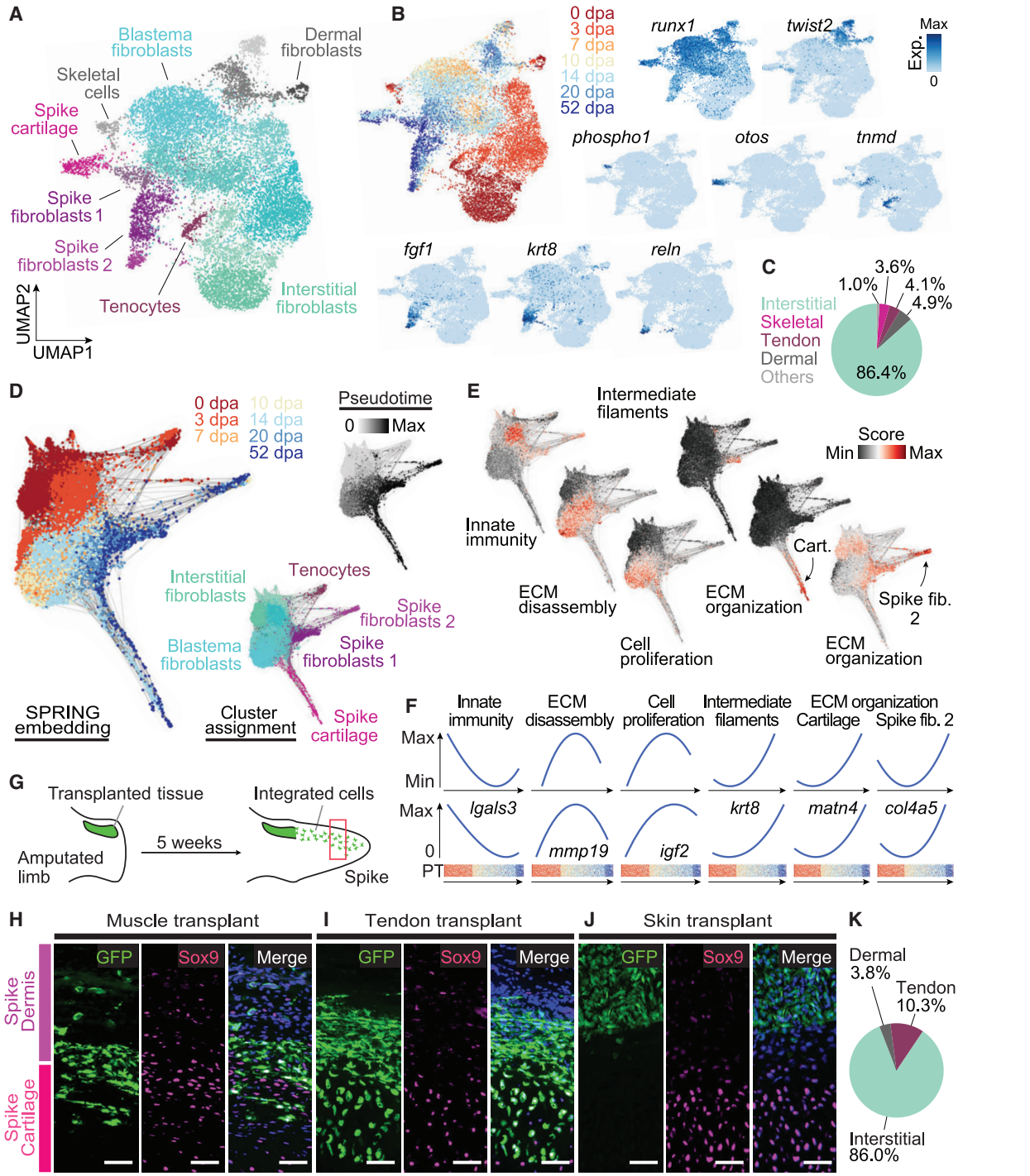

Figure 2. Dermis- and interstitium-derived blastema cells contribute differentially to spike cartilage

(A) UMAP embedding of scRNA-seq data of 15,014 cells from a frog blastema time course after data integration using Harmony (Korsunsky et al., 2019). Cells are colored by cluster and cell type annotations are noted. CT cells shown here were extracted from the blastema cell atlases shown in Figures S1A and 1N, or were experimentally enriched by FACS (0 and 3-dpa cells).

(B) Left: UMAP embedding as shown in (A) with cells being colored by sampling time point. Right and Bottom: feature plots visualizing the expression of cluster marker genes.

(C) Pie chart showing fractions of cell types composing the CT in the mature uninjured state (0 dpa).

(D) Spring plot (Weinreb et al., 2018) of Harmony-integrated scRNA-seq data of 13,124 CT cells excluding skeletal and dermal cells. Left: cells colored by time point. Center: cells are colored by cluster with cell types being noted. Right: cells colored by ranked pseudotime estimates obtained from a diffusion map analysis (Angerer et al., 2016).

(legend continued on next page)

mature interstitial CT and tendon clusters toward spike cartilage and mesenchyme clusters. Interestingly, the dermal cluster was distinct and included cells from all blastema time points, suggesting that, unlike in the case of axolotls, dermal cells do not funnel into the main blastema cluster and therefore do not contribute to spike cartilage and mesenchyme. We next performed a pseudotime analysis to align all CT cells, excluding dermal and skeletal cells, along a regeneration trajectory and visualized the cells in a force-directed layout of a k-nearest neighbor graph (Weinreb et al., 2018) (Figure 2D). We found that interstitial CT and tendon-associated cell types converged to a common phenotype in the early blastema (3 dpa), which then progressed through various blastema stages prior to a bifurcation into spike mesenchyme and spike cartilage around 10 and 14 dpa (Figure 2D). Gene ontology (GO) enrichment analysis for gene sets marking different phases along the pseudotime course revealed the presence of an initial innate immune response followed by signatures of ECM disassembly, cell proliferation, intermediate filaments, and finally, ECM organization (Figures 2E and 2F). Overall, this progression resembles the progression found in axolotls during regeneration (Gerber et al., 2018).

Dermis- and interstitium-derived blastema cells contribute differentially to spike cartilage

To functionally validate the cell trajectory inferences from the single-cell sequencing data, we performed tissue scale transplantations to determine the contributions of bone (periosteum), interstitial-cell-, dermis-, and tendon-derived CT cells to the regenerated spike cartilage (Figures 2G–2J and S2A–S2H). Interestingly, similar to the axolotl, bone-derived CT cells contributed to callus formation at the amputation plane but not significantly to spike outgrowth (Figures S2A and S2B). Tendon or interstitial fibroblast transplants (through muscle transplantation) readily contributed to Sox9-expressing spike cartilage (Figures 2H, 2I, and S2C–S2F). Dermal transplants showed extensive migration in a distinct dermis-like layer at the tip of the blastema with minimal contribution to cartilage (Figures 2J, S2G, and S2H). We carefully examined two samples for each type of transplantations and observed a similar trend in the contribution of donor cells to chondrogenic lineage between samples of the same type (Figure S2I). Quantitation of each tissue's contribution to cartilage (taking into account the proportional representation of each tissue at the amputation plane) revealed that interstitial fibroblasts contributed 85.6% of cells to spike cartilage, whereas tendon- and dermis-derived cells contributed only 10.6% and 3.8%, respectively (Figure 2K; Table S1). These results show that while interstitial, tendon, and dermal CT can contribute to the frog blastema, dermis remains largely as a separate tissue layer with very little, if any, contribution to regenerated cartilage, which contrasts with the successful regeneration in axolotls.

Frog blastema cells show intrinsic limitations in dedifferentiation

These results raised the question of whether frog CT cells are fully reprogrammed to limb bud progenitor potential, as seen in axolotls. To compare axolotl and frog cells, we generated scRNA-seq data for similarly staged axolotl and frog limb buds and blastemas (Figures 3A and S3A–S3D) and used quadratic programing analysis to diagnose to what extent frog blastema cells as compared with axolotl blastema cells acquire a limb bud progenitor identity *in situ*. For each species, we used a set of adult-CT- versus embryonic-limb-bud-specific genes to decompose each cell's identity into a fractional adult and fractional embryonic identity. This analysis showed that between 7 and 14 dpa, frog blastema cells express a fraction of the embryonic limb bud program. However, in contrast to axolotls in which a significant proportion of cells between 11 and 25 dpa approached almost 100% limb bud character, none of the frog cells reached 100%, with a very small fraction reaching a maximum of 60% limb bud identity (Figure 3A). In addition, when integrating limb bud and mature CT cells for each species using Harmony (Korsunsky et al., 2019), the same integration parameters led to a complete mixing of blastema and limb bud cells for axolotls but not for frog CT cells (Figures S3E and S3F). These findings indicated that the adult frog blastema does not fully dedifferentiate to an embryonic-like phenotype *in situ*.

We wanted to further ask whether this incomplete reprogramming was due to an intrinsic restriction within the fibroblasts' potential, or due to limited or even inhibitory environmental cues. We therefore developed a functional assay to test axolotl and frog CT potentials (Figure 3B). Transplantation of frog blastema to axolotl blastema, which would have been ideal, showed rapid tissue rejection (Figures S3G and S3H); therefore, we adopted transplantation into the embryonic limb bud as the test bed to assay regenerative capacities. Upper leg axolotl blastema cells that regain a full embryonic limb bud state should contribute to patterned skeleton, including the foot when transplanted into an axolotl limb bud. If frog blastema cells that show incomplete regeneration are limited by signals in their adult environment but are actually intrinsically capable of regenerating a limb, they should show the same characteristics when transplanted into frog limb buds. On the other hand, if frog CT cells undergo incomplete reprogramming and intrinsically lack the capability of regenerating a limb, their contribution to patterned skeleton in this assay would be limited. We first validated the

(E) GO enrichment scores identified based on genes differentially expressed along the pseudotime course. Scores are visualized as feature on the SPRING embedding. Innate immune response (GO:0045087), extracellular matrix (ECM) disassembly (GO:0022617), Positive regulation of cell proliferation (GO:0008284), Intermediate filament (GO:0005882), ECM organization (GO:0030198).

(F) Top: GO enrichment scores are visualized as a function of pseudotime by a loess fitted curve through the data points. Bottom: expression intensities of example genes for each GO term are shown.

(G) Schematic illustration of tissue transplantation assays. See Figure S2 for details. Red box indicates the regions shown in (H–J).

(H–J) Magnified insets from representative longitudinal sections of muscle (H) (n = 2), tendon (I) (n = 2), and skin (J) (n = 2) transplantation samples. Sections were immunostained for GFP (donor tissue, green), Sox9 (chondrocytes, magenta), and the merged image with DAPI (nuclei, blue). The field of view was further divided into spike dermis (upper region, purple) and spike cartilage (lower region, magenta) according to the expression of Sox9. Scale bars represent 20 μm.

(K) Pie chart showing percentage contributions of interstitial cells, tendon cells and dermal cells to Sox9-expressing cartilage in the spike.

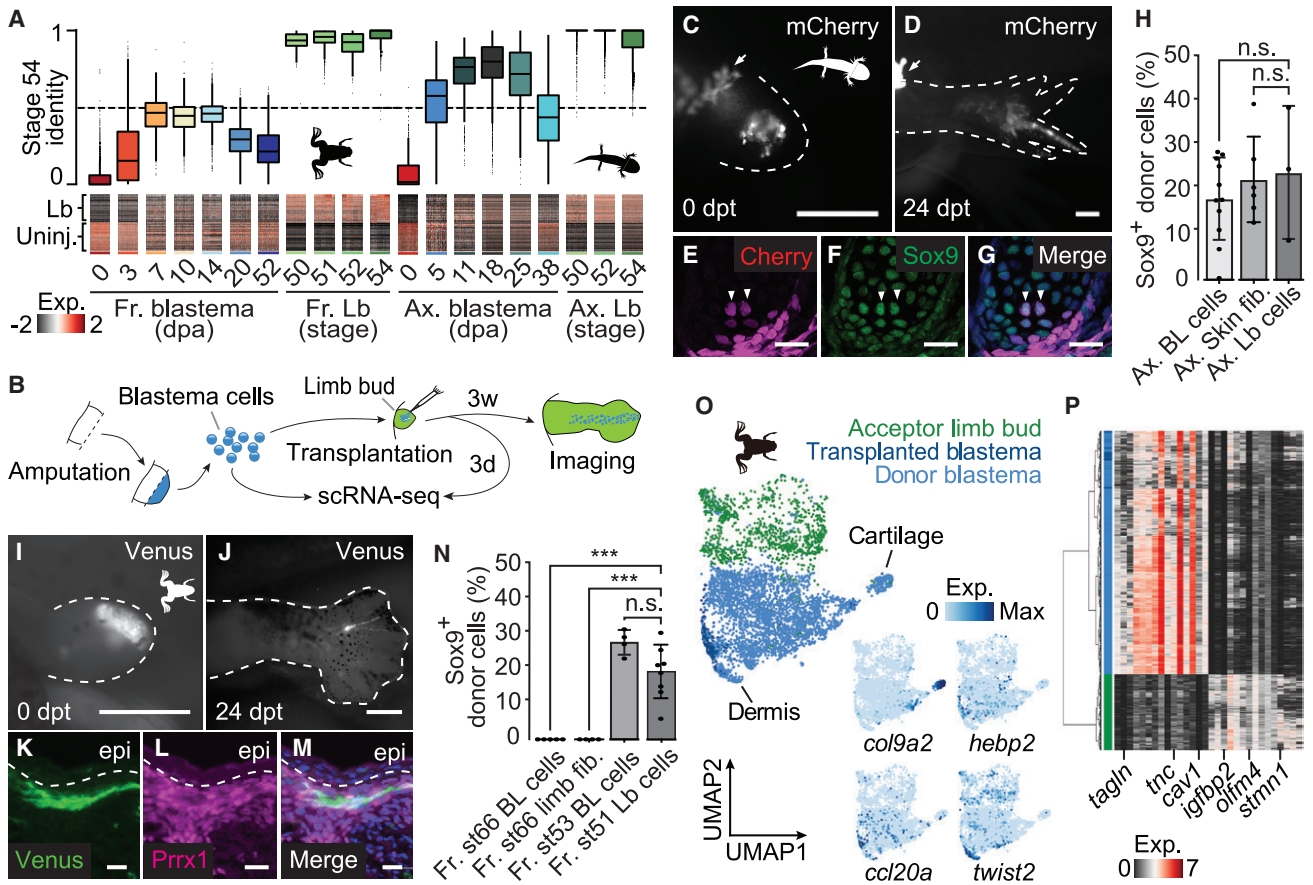

Figure 3. Froglet blastema cells show incomplete reprogramming to a limb-bud-like progenitor state

(A) Quadratic programing shows limited conversion of frog blastema cells to embryonic phenotype. Top: violin plots show fractional embryonic (stage 54) identity in comparison to mature identity for frog (left) and axolotl (right) CT blastema and limb bud cells. See Figures S3E and S3F for cellular heterogeneity. 0 = 100% mature identity; 1 = 100% limb bud identity. Bottom: heatmap representation of scaled gene expression across single cells (columns) for genes (rows) used as input for the quadratic programing analysis in frog and axolotl, respectively. Differences in cell numbers per time point were neglected and genes were sorted by timepoint specificity.

(B) Schematic of the transplantation assay. Unsorted blastema cells of axolotls or froglets were dissociated and injected into developing limb buds of the respective species. For a frog blastema to limb bud transplantation scRNA-seq data was acquired for the donor blastema population and the limb bud cells 3 days after transplantation in addition to imaging data.

(C and D) Fluorescent images of a *d/d* axolotl limb bud 0 day post-transplantation (dpt) (C) and 24 dpt (D) after transplantation of unsorted mCherry-expressing axolotl 9 dpa blastema cells. White dashed lines outline the limb buds. Arrows show non-specific tissue autofluorescence. Scale bars represent 500 μm.

(E–G) Transverse section of (D) at the digit level, immunostained for Cherry (donor cells, magenta) (E), Sox9 (chondrocytes, green) (F), and the merged image with DAPI (nuclei, blue) (G). Arrowheads indicate examples of Cherry$^+$/Sox9$^+$ cells, which are transplanted cells that have integrated into cartilage. Scale bars represent 20 μm.

(H) Bar plot showing the ratio of Sox9-expressing Cherry-positive cells from unsorted axolotl blastema-to-limb bud (Ax. BL cells, n = 11), FAC-sorted axolotl skin fibroblasts-to-limb bud (Ax. Skin fib. n = 6), and unsorted axolotl limb bud-to-limb bud (Ax. Lb cells, n = 3) transplantation experiments. Statistical significance is calculated using unpaired Student's t test. n.s.: $p > 0.05$. Data are represented as mean ± SD.

(I and J) Fluorescent images of a wild-type frog tadpole limb bud 0 dpt (I) and 24 dpt (J) after transplantation of unsorted Venus-expressing frog 14 dpa blastema cells. White dashed lines outline the embryonic limb buds. Scale bars represent 500 μm.

(K–M) Epidermal region of a section of a transplanted frog sample from (J) immunostained for Venus (donor cells, green) (K) and Prrx1 (CT cells, magenta) (L) and the merged image with DAPI (nuclei, blue) (M). Scale bars represent 20 μm.

(N) Bar plot showing the ratio of Sox9-expressing Cherry$^+$ cells from unsorted stage 66 froglet blastema-to-limb bud (Fr. st66 BL cells, n = 5), FAC-sorted stage 66 froglet limb fibroblasts-to-limb bud (Fr. st66 limb fib, n = 4), unsorted stage 53 regenerative limb-bud-blastema-to-limb-bud (Fr. st53 BL cells, n = 4), and unsorted stage 51 frog limb-bud-to-limb-bud (Fr. st51 Lb cells, n = 8) transplantation experiments. Statistical significance is calculated using unpaired Student's t test. ***$p < 0.001$. Data are represented as mean ± SD.

(O) UMAP embedding of scRNA-seq data from the host limb bud acceptor cells (green) and transplanted blastema cells (dark blue) 3 days after transplantation, and blastema donor cells before transplantation (light blue) after data integration using Harmony (Korsunsky et al., 2019). Cells are colored by sample type. Feature plots (right) visualize expression of a cartilage (*col9a2*) and a dermis marker gene (*twist2*) and two transplant-specific genes on the UMAP embedding.

(P) Heatmap shows the expression of main limb bud and donor blastema cluster markers (columns) for cells (rows) shown in (O). Cells were hierarchically clustered using ward.D2. Example genes are highlighted underneath the heatmap.

heterochronic transplantation approach in axolotls by transplanting unsorted, fluorescently labeled 9 dpa upper leg axolotl blastema cells into stage 51-*d/d* axolotl hindlimb buds (Figures 3C and 3D). Transplanted blastema cells contributed to patterned skeleton along the entire proximal-distal axis comparable with transplanted limb bud cell controls (Figures 3E–3H and S4A–S4C). These results reflect acquisition of a multipotent state with a robust contribution to limb development. We then tested the potency of frog blastema cells by transplanting unsorted, fluorescently labeled frog blastema cells into stage 50 wild-type tadpole limb buds (Figures 3I and 3J). Interestingly, while control unsorted frog limb bud cell transplants showed a similar integration profile as in axolotl, indicating comparability of the assays (Figures S4G–S4I), the frog blastema cells did not contribute to the developing skeleton but rather associated with dermis-like elements in the foot (Figures 3K–3N and S4D–S4F). Frog fibroblasts directly dissociated and FAC sorted from the mature limb also showed a similar lack of contribution to developing skeleton (Figures 3N and S4J). The starting number of injected donor cells was comparable across transplantation experiments (Figure S4K). To confirm the competence of the isolated frog blastema cells to integrate with host tissue, we transplanted the unsorted frog blastema cells back into the blastema of thymectomized post-metamorphic hosts where they robustly contributed to the spike (Figures S4L and S4M). To further rule out the possibility that the wound-healing response in frog prohibited the chondrogenic contribution of donor cells in general, we transplanted unsorted blastema cells from regenerative, stage 53 frog limb bud blastemas to stage 50 limb buds (Figures 3N and S4N–S4Q). The blastema cells of the regenerative stage contributed abundantly into host cartilage in a similar fashion compared with the control limb bud transplants (Figures 3N and S4N–S4Q).

These functional experiments point to an incomplete reprogramming of frog CT cells after limb amputation. We next used scRNA-seq on frog donor blastema, host limb bud and transplanted blastema cells to directly measure at the molecular level the extent of reprogramming. In a UMAP embedding of Harmony-integrated data as well as in a hierarchical clustering analysis (Figures 3O and 3P), the transplanted frog blastema cells clustered together with the donor blastema cells rather than the host limb bud cells indicating that they do not acquire the phenotype of surrounding limb bud cells but closely resemble the original blastema donor cells 3 days after transplantation. Only few transplant-specific marker genes could be identified and comprised immune-related genes such as *ccl20a* or necrotic factors such as *hebp2* (Figure 3O). Notably, these genes were also detected in a fraction of blastema cells but not in limb bud cells. In summary, our combined functional and transcriptomic analysis shows that frog blastema cells are incompletely reprogrammed and intrinsically incapable of undertaking a full limb development program.

Frog blastema cells harness a distinct cartilage differentiation program compared with embryonic tadpole limb bud cells

An interesting aspect of our experiments is the capability of adult frog blastema cells to differentiate into a cartilage rod, but their incompetence to contribute to patterned cartilage when transplanted to the limb bud. We therefore compared the cartilage differentiation programs in the frog limb bud (Figures 4A and S4R) and the frog blastema (Figure 4B) at the single-cell transcriptomic level. In both scenarios, differentiation into cartilage cells was defined by expression of cartilage-specific genes including *otos*, *col9a2,* and *matn4*. However, we found a discrepancy in the expression of patterning-related genes such as *meis1*, *hoxa11,* and *hoxa13*. While patterning along the proximal-distal axis in the frog limb bud cartilage was defined by an anticorrelation in expression of the proximal marker *meis1* and the distal markers *hoxa13* and *hoxd13*, no clear correlation or anticorrelation in expression of these genes was detected in cartilage cells of the frog blastema (Figure 4C). In addition, the overall expression levels of these patterning genes were greatly reduced in differentiating cartilage cells in the frog blastema compared with the limb bud (Figures 4D, S4S, and S4T). This shows that the cartilage differentiation program in the frog blastema lacks proper proximal-distal patterning, consistent with previous reports examining selected transcripts (Ohgo et al., 2010). In contrast, we found a clear signature of proximal-distal patterning for differentiating cartilage cells in the axolotl blastema and limb buds (Figures 4E, 4F, and S4U). The deranged *hox* gene expression in the frog blastema is likely functionally linked to the inability of these cells to participate in limb developmental chondrogenesis. Previous work in chicken and mice showed that *hoxa* and *hoxd* genes confer segment-specific chondrocyte condensation and skeletal morphogenesis properties to limb progenitors during development (Boulet and Capecchi, 2004; Fromental-Ramain et al., 1996; Yokouchi et al., 1995).

To further compare cartilage differentiation in different scenarios, we first ordered cells based on a cartilage score, which was calculated using shared cartilage development markers (e.g., *otos*, *col9a2*, see STAR methods for full lists) (Figure 4G), and then performed a differential expression analysis for cells of matching cartilage scores between frog blastema and limb buds. As a comparison, we also performed this analysis on differentiating cartilage cells in axolotl limb bud versus blastema (Figure 4H). We identified various genes that were specifically expressed during cartilage development in the frog limb bud but not in the frog blastema (Figure 4I), including the known cartilage development marker *nog*, the bone mineralization associated gene *irx3*, and the Wnt-pathway-related gene *dact1*. In contrast, *matrilines* (*matn1* and *matn2*) as well as genes associated with cell adhesion (GO:0007155), such as *hapln3* and *edil1*, were only found to be expressed in the frog blastema and not the frog limb bud, highlighting further molecular distinctions in the cartilage differentiation program in the frog blastema compared with the frog limb bud. Remarkably, when we examined the orthologs of these genes in the axolotl, we found that the axolotl limb bud and blastema cartilage cells showed similar expression profiles validating the conclusion that axolotl CT cells attain a bona fide limb-bud-like state in the blastema (Figure 4I). A potential gene network guiding the correct patterning of cartilage in limb buds and the axolotl blastema might be the coordinated expression of *sox8* and *dlx5*, two transcription factors potentially interacting with each other (Wissmüller et al., 2006), that are absent or only weakly expressed in the frog blastema. We found that only a few genes (*rarres1*, *myc*, *pim1*) differentially expressed between axolotl limb bud and blastema cells

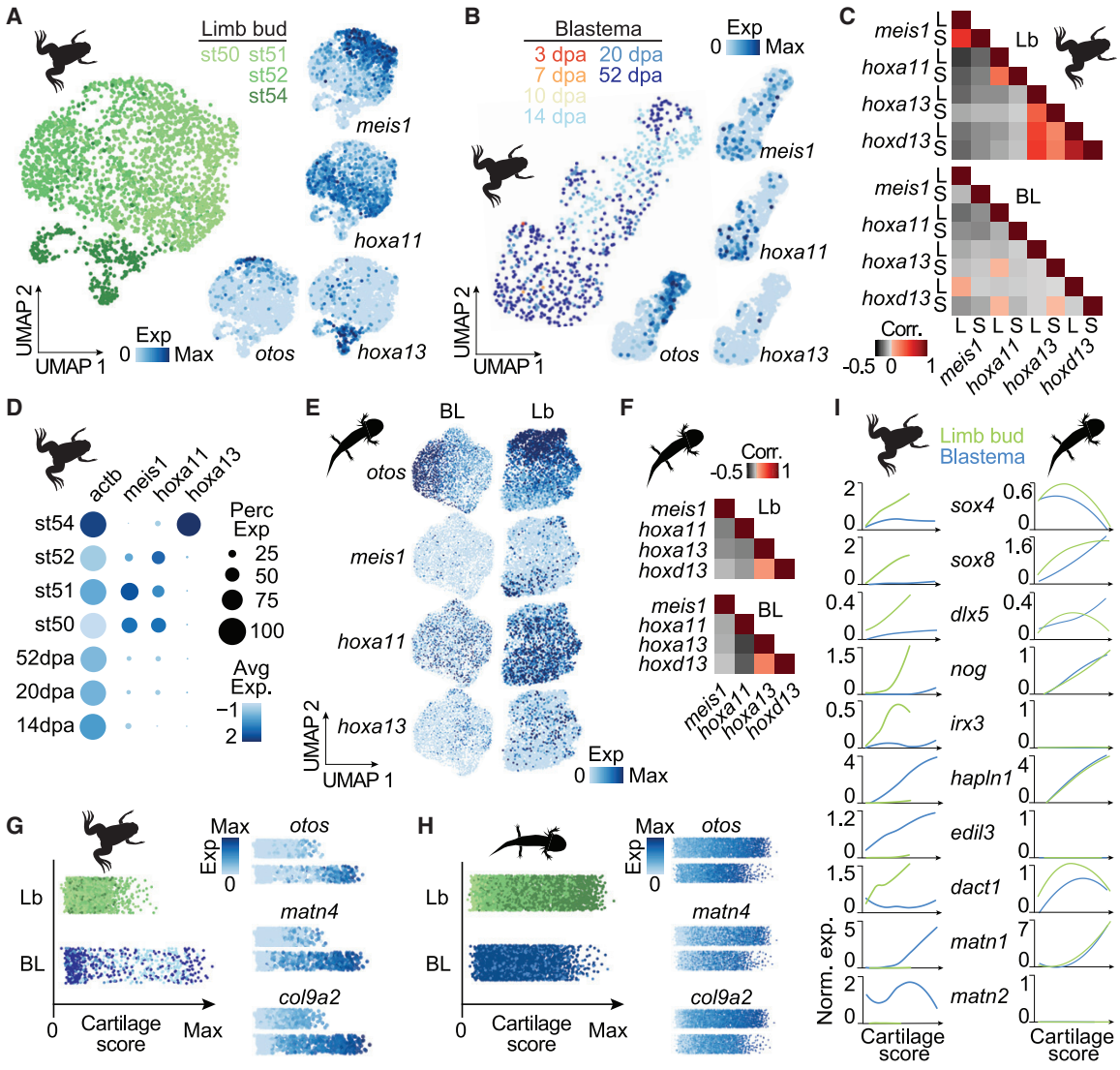

Figure 4. Proximal-distal stratification of patterning factors during cartilage formation in axolotl blastema and tadpole limb buds, but not in froglet blastema

(A) UMAP embedding of scRNA-seq data from limb bud cartilage cells ranging from stage 50 to stage 54 limb buds. Cells are colored by limb bud stages. Feature plots (right) show the expression of maturing cartilage marker (*otos*) and proximal-distal patterning factors (*meis1, hoxa11, hoxa13*). Cartilage cells were isolated based on the clustering of cells in Figure S4R.

(B) UMAP embedding of scRNA-seq data from frog blastema cartilage cells with cartilage cells being isolated based on the clustering of cells in Figure 2A. Cells are colored by blastema time points. Expression of *otos, meis1, hoxa11, and hoxa13* are visualized as feature plots.

(C) Correlation matrix for proximal-distal patterning genes in the developing cartilage of tadpole limb bud (Lb, top) and frog blastema (BL, bottom).

(D) Dot plot showing gene expression intensity and frequency differences between developing cartilage cells in the tadpole limb bud and the frog blastema. Avg Exp: average expression values, Perc Exp: percent of cells expressing each gene. See Figures S4S and S4T for more information.

(E) Feature plots showing expression level of *otos, meis1, hoxa11 and hoxa13* on UMAP embeddings of scRNA-seq data from the cartilage cells of an 18-dpa axolotl blastema (BL, left) and limb buds (Lb, right). Cartilage cells were isolated based on the clustering of cells in Figure S4U.

(F) Correlation matrix for proximal-distal patterning genes in the developing cartilage cells of an 18-dpa axolotl blastema (BL, bottom) and axolotl limb buds (Lb, top).

(G) Cartilage scores (x axis) of frog limb bud (Lb, green) and blastema (BL, blue) cells, respectively, based on common markers of cartilage development (left, see STAR methods). Cells are colored by sample with colors matching the ones in (A) and (B) and are jittered along the y axis. Right: Exemplary feature plots of common cartilage development markers.

(H) Cartilage scores (x axis) of axolotl limb bud (Lb, green) and blastema (BL, blue) cells, respectively, based on common markers of cartilage development (left, see STAR methods). Cells are colored by sample with colors matching the ones in Figure S4U and are jittered along the y axis. Right: exemplary feature plots of common cartilage development markers.

(I) Gene expression as a function of cartilage score for selected genes identified to be differentially expressed between frog limb bud and blastema cartilage differentiation is visualized for frog (left) and axolotl (right) limb bud and blastema cartilage cells. A loess fitted curve through the data points is shown. Green: limb bud. Blue: blastema.

(Figure S4V) and these genes did not show similar expression curves in the corresponding frog tissues. Only one gene, *adrenomedullin 2* (*adm2*), showed a consistently high expression in the blastema compared with limb bud for frog and axolotl, suggesting a blastema specific role in cartilage development not needed in embryonic limb buds.

DISCUSSION

To understand how frogs fail to regenerate a fully patterned limb, it is essential (1) to study the cellular and molecular mechanisms underlying the abortive regeneration process, (2) to compare these mechanisms to a successful model of limb regeneration, and (3) to test which of the differences that we find between the two models that could account for the regeneration failure. Here, by establishing previously unavailable methods, such as lineage tracing with a stable transgenic CreERT/LoxP line, single-cell RNA-seq, and a transplantation-based functional assay, we systematically compared the differences between the limb regeneration processes of frogs and axolotls.

One previously unresolved question is whether the frog blastema is composed of similar cell types and derives from a similar origin as blastema cells in the axolotl. A rigorous treatment of this question requires genetic fate mapping of candidate source tissues. To date, only a doxycycline-inducible labeling system targeting tadpole chondrogenic cells was reported (Mochii et al., 2007), and an attempt to label tadpole trunk and leg muscles using the CreERT/LoxP system was unsuccessful (Rodrigues et al., 2012). Here, we successfully established *Prrx1:CreER;-CAGGs:lp-Cherry* stable transgenic frog lines that allow conditional labeling and tracing of limb CT cells. Combining lineage tracing with both single-cell RNA-seq analysis and immunostaining, we confirmed that, similar to an axolotl blastema, the frog blastema is composed of a comparable proportion of soft connective tissue-derived fibroblasts (Figure 1). Our scRNA-seq result also suggests that there is no pre-existing stem cell pool in frog limbs.

In contrast, frog blastema cells behave differently compared with axolotl blastema cells at the molecular level. Unlike axolotl dermal fibroblasts, which undergo dedifferentiation and contribute to multiple CT types, frog dermal fibroblasts maintained their dermal identity throughout the regeneration process. In addition, even though frog interstitium-derived blastema fibroblasts progressed through similar phases as axolotl blastema cells based on a GO enrichment analysis of the regeneration time course (Figures 2E and 2F; Gerber et al., 2018), they did not fully dedifferentiate to limb-bud-like progenitors before they differentiated into chondrocytes (Figure 3A). According to morphological data and bulk transcriptomic analysis, axolotl regeneration proceeds through 3 distinct stages: wound healing, blastema formation (dedifferentiation), and re-development (patterning) (Bryant et al., 2002; Knapp et al., 2013). Due to its unbranched and unsegmented appearance, the frog spike phenotype has long been regarded as a patterning defect (Suzuki et al., 2006). Our observation, however, suggests that the frog spike phenotype is not merely a patterning problem but rather an outcome of incomplete dedifferentiation prior to patterning. It is important to identify missing factors and/or pathways during frog limb regeneration, and to develop tools to determine whether complete dedifferentiation could lead to complete patterning in future studies. Our single-cell transcriptomic comparison of cartilage formation in the limb bud versus the limb blastema also points to molecular distinctions between the two processes above and beyond the very noticeable suppression and derangement of the patterning program.

To date, rescuing the spike phenotype by ectopically applying or expressing extracellular factors, such as *fgf* (fibroblast growth factor), *bmp* (bone morphogenic protein), *shh* (sonic hedgehog), and progesterone, has been a main focus of the field (Herrera-Rincon et al., 2018; Lin et al., 2013; Mitogawa et al., 2018; Satoh et al., 2005; Yakushiji et al., 2009). The assumption behind this strategy is that frog blastema cells have capacities to correctly respond to extrinsic signals, and thus, the environmental cues are the determinants for successful limb regeneration. While our result does not exclude the importance of extracellular factors, it strongly suggests that cell intrinsic, most likely epigenetic, limitations are the key hinderance to complete regeneration. Characterizing and overcoming those epigenetic limitations will be crucial to improve regeneration in future studies.

In summary, our findings have important implications for regenerative medicine as they show that generic chondrogenic or osteogenic potential (i.e., *in vitro* differentiation) is an insufficient criterium for regenerative potential *in vivo* when aiming to rebuild functional skeleton. Strategies to restore embryonic, position-appropriate qualities to CT descendants should become a major focus of future regenerative medicine efforts.

Limitations of the study

Although our heterochronic transplantation experiments distinguished between the cell intrinsic potency of frog and axolotl limb blastema cells, we cannot completely rule out the possibility that the dedifferentiation observed in axolotl blastema is directed by ''regeneration inducers'' in the axolotl limb environment that are not present in the frog. Such hypothetical inducers, either secreted, circulating, and/or ECM molecules, could potentiate axolotl limb fibroblasts and push the cells through the dedifferentiation process. Ideally, transplanting frog fibroblasts into the axolotl limb blastema would be an elegant way to test this hypothesis. Unfortunately, we were not able to establish such assays in this study due to the rapid rejection of frog donor cells (Figure S3G). Similar results were obtained when using thymectomized axolotls as hosts (data not shown), suggesting that mechanisms other than immune rejection, such as the incompatibility of growth factors, might play roles in the failure of integration. Overcoming the compatibility problem would be a valuable direction in future studies.

STAR★METHODS

Detailed methods are provided in the online version of this paper and include the following:

- KEY RESOURCES TABLE
- RESOURCE AVAILABILITY
  - Lead contact
  - Materials availability
  - Data and code availability
- EXPERIMENTAL MODEL AND SUBJECT DETAILS

SUPPLEMENTAL INFORMATION

Supplemental information can be found online at https://doi.org/10.1016/j.devcel.2021.04.016.

ACKNOWLEDGMENTS

We thank the animal care team at the Vienna Biocenter and CRTD Dresden for great animal care and breeding, and all the members of the Tanaka and Treutlein labs for helpful discussions. We thank Nicole Ziegler and Eva Kania for technical assistance. We thank previous lab members Shahryar Khattak, Annette Duemmler, and Tobias Richter for making CAGGs:mTFP1 and CAGGs:mCherry constructs. Crystalin promoter sequence was kindly provided by Professor Daniel L. Weeks in the Department of Biochemistry, University of Iowa. We thank Leo Otsuki for discussion and proofreading the manuscript. We thank the VBCF NGS facility and the IMP Bio-Optics and MBS facilities for outstanding service. Animal experiments were performed as approved by the Magistrate of Vienna and the State Authorities Saxony. Funding: E.M.T. was supported by core funds of the IMP; DFG FZT 111, Germany; ERC AdG 294324 RegenerateAcross and 742046 RegGeneMems, European Union. B.T. was supported by core funds of the Max Planck Society, Germany; ETH Zürich, Switzerland; and ERC StG 758877 Organomics, European Union.

AUTHOR CONTRIBUTIONS

T.-Y.L. and S.H. generated transgenic *Xenopus laevis* lines with assistance from P.M. T.-Y.L. and L.G. performed cell transplantation experiments. Y.T.-S. performed tissue scale transplantation experiments. E.S. performed cross-species blastema transplantation experiments. T.-Y.L., S.H., and Y.T.-S. performed immunohistochemistry. T.-Y.L. and T.G. performed single-cell experiments. T.G. analyzed scRNA-seq data. T.-Y.L., T.G., Y.T.-S., B.T., and E.M.T. designed the study, analyzed data, and wrote the manuscript.

DECLARATION OF INTERESTS

E.M.T. is a member of the advisory board for developmental cell but did not participate in the editorial process of this manuscript.

Received: September 6, 2020
Revised: February 3, 2021
Accepted: April 16, 2021
Published: May 17, 2021

REFERENCES

Angerer, P., Haghverdi, L., Büttner, M., Theis, F.J., Marr, C., and Buettner, F. (2016). destiny: diffusion maps for large-scale single-cell data in R. Bioinformatics *32*, 1241–1243.

Aztekin, C., Hiscock, T.W., Gurdon, J.B., Jullien, J., Marioni, J.C., and Simons, B.D. (2020). Secreted inhibitors drive the loss of regeneration competence in Xenopus limbs. bioRxiv. https://doi.org/10.1101/2020.06.01.127654.

Bankhead, P., Loughrey, M.B., Fernández, J.A., Dombrowski, Y., McArt, D.G., Dunne, P.D., McQuaid, S., Gray, R.T., Murray, L.J., Coleman, H.G., et al. (2017). QuPath: open source software for digital pathology image analysis. Sci. Rep. *7*, 16878.

Boulet, A.M., and Capecchi, M.R. (2004). Multiple roles of Hoxa11 and Hoxd11 in the formation of the mammalian forelimb zeugopod. Development *131*, 299–309.

Bryant, S.V., Endo, T., and Gardiner, D.M. (2002). Vertebrate limb regeneration and the origin of limb stem cells. Int. J. Dev. Biol. *46*, 887–896.

Butler, A., Hoffman, P., Smibert, P., Papalexi, E., and Satija, R. (2018). Integrating single-cell transcriptomic data across different conditions, technologies, and species. Nat. Biotechnol. *36*, 411–420.

Dobin, A., Davis, C.A., Schlesinger, F., Drenkow, J., Zaleski, C., Jha, S., Batut, P., Chaisson, M., and Gingeras, T.R. (2013). STAR: ultrafast universal RNA-seq aligner. Bioinformatics *29*, 15–21.

Fromental-Ramain, C., Warot, X., Lakkaraju, S., Favier, B., Haack, H., Birling, C., Dierich, A., Doll e, P., and Chambon, P. (1996). Specific and redundant functions of the paralogous Hoxa-9 and Hoxd-9 genes in forelimb and axial skeleton patterning. Development *122*, 461–472.

Gerber, T., Murawala, P., Knapp, D., Masselink, W., Schuez, M., Hermann, S., Gac-Santel, M., Nowoshilow, S., Kageyama, J., Khattak, S., et al. (2018). Single-cell analysis uncovers convergence of cell identities during axolotl limb regeneration. Science *362*, eaaq0681.

Haghverdi, L., Büttner, M., Wolf, F.A., Buettner, F., and Theis, F.J. (2016). Diffusion pseudotime robustly reconstructs lineage branching. Nat. Methods *13*, 845–848.

Harty, M., Neff, A.W., King, M.W., and Mescher, A.L. (2003). Regeneration or scarring: an immunologic perspective. Dev. Dyn. *226*, 268–279.

Herrera-Rincon, C., Golding, A.S., Moran, K.M., Harrison, C., Martyniuk, C.J., Guay, J.A., Zaltsman, J., Carabello, H., Kaplan, D.L., and Levin, M. (2018). Brief local application of progesterone via a wearable bioreactor induces long-term regenerative response in adult Xenopus Hindlimb. Cell Rep *25*, 1593–1609.e7.

Horton, J.D., Horton, T.L., Dzialo, R., Gravenor, I., Minter, R., Ritchie, P., Gartland, L., Watson, M.D., and Cooper, M.D. (1998). T-cell and natural killer cell development in thymectomized Xenopus. Immunol. Rev. *166*, 245–258.

Huang, da W., Sherman, B.T., and Lempicki, R.A. (2009). Systematic and integrative analysis of large gene lists using DAVID bioinformatics resources. Nat. Protoc. *4*, 44–57.

Karimi, K., Fortriede, J.D., Lotay, V.S., Burns, K.A., Wang, D.Z., Fisher, M.E., Pells, T.J., James-Zorn, C., Wang, Y., Ponferrada, V.G., et al. (2018). Xenbase: a genomic, epigenomic and transcriptomic model organism database. Nucleic Acids Res *46*, D861–D868.

Khattak, S., Murawala, P., Andreas, H., Kappert, V., Schuez, M., Sandoval-Guzmán, T., Crawford, K., and Tanaka, E.M. (2014). Optimized axolotl (Ambystoma mexicanum) husbandry, breeding, metamorphosis, transgenesis and tamoxifen-mediated recombination. Nat. Protoc. *9*, 529–540.

Khattak, S., Schuez, M., Richter, T., Knapp, D., Haigo, S.L., Sandoval-Guzmán, T., Hradlikova, K., Duemmler, A., Kerney, R., and Tanaka, E.M. (2013). Germline transgenic methods for tracking cells and testing gene function during regeneration in the axolotl. Stem Cell Rep *1*, 90–103.

King, M.W., Neff, A.W., and Mescher, A.L. (2012). The developing Xenopus limb as a model for studies on the balance between inflammation and regeneration. Anat. Rec. (Hoboken) *295*, 1552–1561.

Knapp, D., Schulz, H., Rascon, C.A., Volkmer, M., Scholz, J., Nacu, E., Le, M., Novozhilov, S., Tazaki, A., Protze, S., et al. (2013). Comparative transcriptional profiling of the axolotl limb identifies a tripartite regeneration-specific gene program. PLoS One *8*, e61352.

Korsunsky, I., Millard, N., Fan, J., Slowikowski, K., Zhang, F., Wei, K., Baglaenko, Y., Brenner, M., Loh, P.R., and Raychaudhuri, S. (2019). Fast, sensitive and accurate integration of single-cell data with Harmony. Nat. Methods *16*, 1289–1296.

Kragl, M., Knapp, D., Nacu, E., Khattak, S., Maden, M., Epperlein, H.H., and Tanaka, E.M. (2009). Cells keep a memory of their tissue origin during axolotl limb regeneration. Nature *460*, 60–65.

Kroll, K.L., and Amaya, E. (1996). Transgenic Xenopus embryos from sperm nuclear transplantations reveal FGF signaling requirements during gastrulation. Development *122*, 3173–3183.

Lin, G., Chen, Y., and Slack, J.M. (2013). Imparting regenerative capacity to limbs by progenitor cell transplantation. Dev. Cell *24*, 41–51.

McCusker, C., Bryant, S.V., and Gardiner, D.M. (2015). The axolotl limb blastema: cellular and molecular mechanisms driving blastema formation and limb regeneration in tetrapods. Regeneration (Oxf) *2*, 54–71.

Mescher, A.L., Neff, A.W., and King, M.W. (2013). Changes in the inflammatory response to injury and its resolution during the loss of regenerative capacity in developing Xenopus limbs. PLoS One *8*, e80477.

Mitogawa, K., Makanae, A., and Satoh, A. (2018). Hyperinnervation improves Xenopus laevis limb regeneration. Dev. Biol. *433*, 276–286.

Mochii, M., Taniguchi, Y., and Shikata, I. (2007). Tail regeneration in the Xenopus tadpole. Dev. Growth Differ. *49*, 155–161.

Muneoka, K., Fox, W.F., and Bryant, S.V. (1986). Cellular contribution from dermis and cartilage to the regenerating limb blastema in axolotls. Dev. Biol. *116*, 256–260.

Nieuwkoop, P.D., and Faber, J. (1956). Normal Table of Xenopus Laevis (Daudin); a Systematical and Chronological Survey of the Development from the Fertilized Egg Till the End of Metamorphosis (North-Holland Publishing).

Nowoshilow, S., and Tanaka, E.M. (2020). Introducing www.axolotl-omics.org - an integrated -omics data portal for the axolotl research community. Exp. Cell Res. *394*, 112143.

Ohgo, S., Itoh, A., Suzuki, M., Satoh, A., Yokoyama, H., and Tamura, K. (2010). Analysis of hoxa11 and hoxa13 expression during patternless limb regeneration in Xenopus. Dev. Biol. *338*, 148–157.

R Core Team (2019). R: A language and environment for statistical computing (Vienna, Austria: R Foundation for Statistical Computing). https://www.R-project.org/.

Rodrigues, A.M., Christen, B., Martí, M., and Izpisúa Belmonte, J.C. (2012). Skeletal muscle regeneration in Xenopus tadpoles and zebrafish larvae. BMC Dev. Biol. *12*, 9.

Satoh, A., Suzuki, M., Amano, T., Tamura, K., and Ide, H. (2005). Joint development in Xenopus laevis and induction of segmentations in regenerating froglet limb (spike). Dev. Dyn. *233*, 1444–1453.

Schloissnig, S., Kawaguchi, A., Nowoshilow, S., Falcon, F., Otsuki, L., Tardivo, P., Timoshevskaya, N., Keinath, M.C., Smith, J.J., Voss, S.R., and Tanaka, E.M. (2021). The giant axolotl genome uncovers the evolution, scaling, and transcriptional control of complex gene loci. Proc. Natl. Acad. Sci. USA *118*. e2017176118. https://doi.org/10.1073/pnas.2017176118.

Sessions, S.K., and Bryant, S.V. (1988). Evidence that regenerative ability is an intrinsic property of limb cells in Xenopus. J. Exp. Zool. *247*, 39–44.

Simon, A., and Tanaka, E.M. (2013). Limb regeneration. Wiley Interdiscip. Rev. Dev. Biol. *2*, 291–300.

Sive, H.L., Grainger, R.M., and Harland, R.M. (2000). Early Development of Xenopus laevis: A Laboratory Manual (Cold Spring Harbor Laboratory Press).

Sobkow, L., Epperlein, H.H., Herklotz, S., Straube, W.L., and Tanaka, E.M. (2006). A germline GFP transgenic axolotl and its use to track cell fate: dual origin of the fin mesenchyme during development and the fate of blood cells during regeneration. Dev Biol *290*, 386–397.

Suzuki, M., Yakushiji, N., Nakada, Y., Satoh, A., Ide, H., and Tamura, K. (2006). Limb regeneration in Xenopus laevis froglet. ScientificWorldJournal *6* (suppl 1), 26–37.

Weinreb, C., Wolock, S., and Klein, A.M. (2018). SPRING: a kinetic interface for visualizing high dimensional single-cell expression data. Bioinformatics *34*, 1246–1248.

Wissmüller, S., Kosian, T., Wolf, M., Finzsch, M., and Wegner, M. (2006). The high-mobility-group domain of Sox proteins interacts with DNA-binding domains of many transcription factors. Nucleic Acids Res *34*, 1735–1744.

Yakushiji, N., Suzuki, M., Satoh, A., Ide, H., and Tamura, K. (2009). Effects of activation of hedgehog signaling on patterning, growth, and differentiation in Xenopus froglet limb regeneration. Dev. Dyn. *238*, 1887–1896.

Yakushiji, N., Suzuki, M., Satoh, A., Sagai, T., Shiroishi, T., Kobayashi, H., Sasaki, H., Ide, H., and Tamura, K. (2007). Correlation between Shh expression and DNA methylation status of the limb-specific Shh enhancer region during limb regeneration in amphibians. Dev. Biol. *312*, 171–182.

Yokouchi, Y., Nakazato, S., Yamamoto, M., Goto, Y., Kameda, T., Iba, H., and Kuroiwa, A. (1995). Misexpression of Hoxa-13 induces cartilage homeotic transformation and changes cell adhesiveness in chick limb buds. Genes Dev *9*, 2509–2522.

Zhang, M., Chen, Y., Xu, H., Yang, L., Yuan, F., Li, L., Xu, Y., Chen, Y., Zhang, C., and Lin, G. (2018). Melanocortin receptor 4 signaling regulates vertebrate limb regeneration. Dev. Cell *46*, 397–409.e5.

STAR★METHODS

KEY RESOURCES TABLE

REAGENT or RESOURCE	SOURCE	IDENTIFIER
Antibodies		
rabbit anti-GFP	Rockland	Cat# 600-401-215; RRID: AB_828167
mouse anti-GFP	MPI-CBG protein facility, Dresden	Cat# 106-A20-Mix
goat anti-mCherry	Acris Antibodies	Cat# AB0040-200; RRID: AB_2333092
Rabbit anti-RFP	Rockland	Cat# 600-401-379; RRID: AB_2209751
rabbit anti-Sox9	Chemicon	Cat# Ab5535; RRID: AB_2239761
goat anti-Sox9	R&D Systems	Cat# AF3075; RRID: AB_2194160
rabbit anti-Prrx1	Gerber et al., 2018	N/A
mouse anti-Pax7	MPI-CBG protein facility, Dresden	AB-022
mouse Anti-Col1A2	Developmental Studies Hybridoma bank	Cat# SP1.D8; RRID: AB_528438
Donkey anti-mouse Alexa 488	Invitrogen	Cat# A-21202; RRID: AB_141607
Donkey anti-mouse Alexa 568	Invitrogen	Cat# A-10037; RRID: AB_2534013
Donkey anti-rabbit Alexa 568	Invitrogen	Cat# A-10042; RRID: AB_2534017
Donkey anti-rabbit Alexa 647	Invitrogen	Cat# A-31573; RRID: AB_2536183
Donkey anti-goat Alexa 568	Invitrogen	Cat# A-11057; RRID: AB_2534104
Donkey anti-goat Alexa 647	Invitrogen	Cat# A-21447; RRID: AB_2535864
Chemicals, peptides, and recombinant proteins		
DAPI	Sigma-Aldrich	Cat# D9542
Mowiol 4-88	Sigma-Aldrich	Cat# 9002-89-5
4-hydroxytamoxifen	Sigma-Aldrich	Cat# 7940
DMSO	Sigma-Aldrich	Cat# D2650
tricaine methanesulfonate (MS222)	Sigma-Aldrich	Cat# A5040
Benzocaine	Sigma-Aldrich	Cat# E1501
pregnant mare serum gonadotropin	ProSpec	Cat# HOR-272
human chorionic gonadotropin	Sigma-Aldrich	Cat# CG10
Liberase TM	Roche	Cat# 5401127001
DNase I	Roche	Cat# 4716728001
OCT compound	Science Service	Cat# 62550-12
Critical commercial assays		
QIAGEN Maxi kit	Qiagen	Cat# 12163
Chromium Single Cell 3′ GEM, Library & Gel Bead Kit v3, 16 rxns	10X Genomics	Cat# PN-1000075
Chromium Chip B Single Cell Kit, 48 rxns	10X Genomics	Cat# PN-1000073
Chromium i7 Multiplex Kit, 96 rxns	10X Genomics	Cat# PN-120262
SPRIselect	Beckman Coulter	Cat# B23318
Bioanalyzer High Sensitivity DNA Kit	Agilent	Cat# 5067-4626
Deposited data		
Raw and analyzed data	This paper	GEO: GSE165901
Xenopus reference genome NCBI build v9.2, Xenbase v9.2 gene models	Xenbase	http://www.xenbase.org/other/static-xenbase/ftpDatafiles.jsp
Axolotl reference genome	Nowoshilow and Tanaka, 2020	www.axolotl-omics.org
Experimental models: organisms/strains		
Xenopus laevis: wildtype	NASCO	Cat# LM00531 (Female); Cat# LM00715 (Male); RRID: XEP_Xla100
Xenopus laevis: wildtype	EXRC	N/A

(*Continued on next page*)

Continued

REAGENT or RESOURCE	SOURCE	IDENTIFIER
Xenopus laevis: CAGGs:Venus	EXRC	RRID: EXRC_0048
Xenopus laevis: CMV:tdTomato	EXRC	RRID: EXRC_0033
Xenopus laevis: CAGGs:nucTFP	This paper	N/A
Xenopus laevis: CAGGs:mCherry	This paper	N/A
Xenopus laevis: CAGGs:lp-Cherry	This paper	N/A
Xenopus laevis: Prrx1:CreER	This paper	N/A
Ambystoma mexicanum: d/d	IMP animal facility	N/A
Ambystoma mexicanum: CAGGs:mCherry	This paper	N/A
Ambystoma mexicanum: CAGGs:GFP	Sobkow et al., 2006	N/A
Oligonucleotides		
Primer Crystallin 5' forward:ACGCGTGG ATCACCTGAAAGCAGGTTG	This paper	N/A
Primer Crystallin 3' reverse:CAGCTCC TCGCCCTTGCTCACCATGGTGG CGCCTAGGTGGCGACCGGTGGATCC	This paper	N/A
Primer mCherry 5' forward: GTGAGCAAGGGCGAGGAG	This paper	N/A
Primer mCherry 3' reverse: CTTGTACAGCTCGTCCATGCC	This paper	N/A
Primer SV40pA 5' forward: GGCAT GGACGAGCTGTACAAGTAACACGT GCTGATCATAATCAGCCATAC	This paper	N/A
Primer SV40pA 3' reverse: GGGCCCGGAATTGCGTTAAGATAC	This paper	N/A
Recombinant DNA		
pMAT/X(TFPnls-T2A-Cre-hERT2)	GeneArt	N/A
CAGGs:nucTFP	This paper	N/A
CAGGs:mCherry	This paper	N/A
CAGGs:loxp-GFP-loxp-mCherry	Khattak et al., 2013	N/A
Crystallin:mCherry; mPrrx1:xen(TFPnls-T2A-Cre-ERT2)	This paper	N/A
Plasmid: CL EGFP DI attB	Daniel L. Weeks Lab, Department of Biochemistry, University of Iowa	N/A
Software and algorithms		
Fiji version 2.1.0/1.53c	Fiji	RRID: SCR_002285
QuPath	Bankhead et al. 2017	RRID: SCR_018257
Zen 3.2 (blue edition)	Zeiss	RRID: SCR_013672
Prism version 9.0.2	GraphPad Software	RRID: SCR_002798
Cellranger 3.1	10xGenomics	RRID: SCR_017344
STARsolo v2.7.5a	Dobin et al., 2013	N/A
R v3.6	R Core Team, 2019	N/A
Other		
Filcon, sterile, (size: 10 μm)	BD bioscience	Cat# 340732
MACS SmartStrainers: 70 μm	Miltenyi Biotec	Cat# 130-098-45
MACS SmartStrainers: 30 μm	Miltenyi Biotec	Cat# 130-098-462
Chromium Controller	10X Genomics	Cat# 1000204; RRID: SCR_019326

RESOURCE AVAILABILITY

Lead contact

Further information and requests for resources and reagents should be directed to and will be fulfilled by the Lead Contact, Elly M. Tanaka (elly.tanaka@imp.ac.at).

Materials availability

All the plasmids and transgenic frog lines generated in this study are available upon request.

Data and code availability

The accession number for the mapped bam files and gene/cell matrix files reported in this paper is GEO: GSE165901. R scripts used for the scRNA-seq analysis are available upon request.

EXPERIMENTAL MODEL AND SUBJECT DETAILS

Xenopus strains and maintenance

Wildtype frogs were obtained from the European Xenopus Resource Center (EXRC), UK and NASCO, USA. Transgenic lines (*CAGGs:Venus* (EXRC line #33) and *CMV:tdTomato* (EXRC line #48) were obtained from EXRC. Frog transgenic lines (*CAGGs:-nucTFP*, *CAGGs:mCherry*, and *Prrx1:CreER;CAGGs:lp-Cherry*) were generated in CRTD animal facilities. All lines were bred and group housed in CRTD and IMP facilities. All animal handling and surgical procedures were carried out in accordance with local ethics committee guidelines. Animal experiments were performed as approved by the State Authorities Saxony and the Magistrate of Vienna. Animals were anesthetized either in 0.003% benzocaine (Sigma-Aldrich, E1501), or 0.03% tricaine methanesulfonate (MS222, Sigma-Aldrich, A5040) before amputation and surgery. *Xenopus laevis* husbandry followed the guidelines as described (Sive et al., 2000). In brief, the female and the male were injected with 500 IU and 50 UI of human chorionic gonadotropin (hCG, Sigma-Aldrich, CG10), respectively, before natural mating. The pair were put together in 7L 20mM NaCl in room temperature overnight. The embryos were collected for the next two days before the mating pair was separated. To obtain frog eggs for transgenesis, wildtype females were primed with 50 IU of pregnant mare serum gonadotropin (PMSG, ProSpec, HOR-272) one week before the injection of 500 IU of human chorionic gonadotropin (hCG, Sigma-Aldrich, CG10) in the evening before egg collection. For surgical experiments in this study, frogs were used at the juvenile stage (see Method details for more information) and were not biased toward specific sex.

Axolotl strains and maintenance

White (*d/d*) axolotls were used as the host of transplantation experiments. The *CAGGs:GFP* axolotl line was previously described (Sobkow et al., 2006), and the *CAGGs:Cherry* axolotl line was established previously in the lab. All lines were bred and maintained in CRTD and IMP facilities and each animal is kept individually. All the handling and surgical procedures were carried out in accordance with local ethics committee guidelines. Animal experiments were performed as approved by the State Authorities Saxony and the Magistrate of Vienna. Animals were anesthetized in 0.003% benzocaine (Sigma-Aldrich, E1501) before amputation and surgery. Axolotl husbandry was described in detail in a previous paper (Khattak et al., 2014). For surgical experiments in this study, axolotls were used at the juvenile stage (see Method details for more information) and were not biased toward specific sex.

METHOD DETAILS

Codon optimization and molecular cloning

TFPnls-T2A-Cre-ERT2 cassette was codon-optimized based on the codon usage of *Xenopus laevis* (GeneArt). To replace the original TFPnls-T2A-Cre-ERT2 cassette, the codon-optimized cassette (xen(TFPnls-T2A-Cre-ERT2)) was subcloned into the Prrx1:CreER construct (Gerber et al., 2018) with restriction enzymes NheI and EcoRI. Fragments of the Crystallin:mCherry cassette (Crystallin promoter, mCherry, SV40 poly-A sequences) was assembled using over-extension PCR before subcloned into the Prrx1:CreER construct using restriction enzymes ApaI and MluI. The reporter CAGGs:lp-GFP-3pA-lp-mCherry-pA construct was described previously (Khattak et al., 2013). All plasmids used in transgenesis were prepared with QIAGEN Maxi kit (Qiagen, 12163)

Transgenesis and 4-hydroxytamoxifen treatment

CAGGs:nucTFP and *CAGGs:mCherry* transgenic *Xenopus laevis* lines were established independently using REMI protocol (Kroll and Amaya, 1996) using existing plasmids in the lab. *Crystallin:mCherry;Prrx1:xen(TFPnls-T2A-Cre-ERT2)-pA* (*Prrx1:CreER* in short) and *CAGGs:loxp-GFP-3pA-loxp-mCherry-pA* (*CAGGs:lp-Cherry* in short) transgenic *Xenopus laevis* lines were generated independently using REMI protocol (Kroll and Amaya, 1996). *Prrx1:CreER* and *CAGGs:lp-Cherry* F0 transgenic tadpoles were screened by virtue of red lens and green trunk muscle, respectively. *Prrx1:CreER*;*CAGGs:lp-Cherry* double positive F1 embryos were treated with 1μM 4-hydroxytamoxifen (4-OHT, Sigma-Aldrich, H7940) overnight at 9-, 11- and 13-days post-fertilization (dpf), and were screened for mCherry signals in the limb bud around stage 50 (42 dpf) to assess conversion efficiency and specificity.

Thymectomy

To suppress the potential immune response of frogs in allograft transplantations, we developed a thymectomy method similar to a published method (Horton et al., 1998; Lin et al., 2013). In brief, tadpoles younger than stage 47 were anesthetized and their thymus glands were removed using surgical scissors and forceps (Fine science tools, 15000-08 and 11251-35). The animals were raised and used as hosts for cell transplantation and bulk tissue grafting mentioned below.

Bulk tissue grafting

For bulk tissue grafting, both Venus$^+$ transgenic donor and thymectomised wild-type host froglets were anesthetized in 0.03% MS-222. For bone transplantations, tibio-fibula were isolated from Venus$^+$ transgenic froglets. To remove the surrounding tissue, isolated bone was treated with Liberase solution for 20 minutes at 37 degrees (15μl of Liberase TM (Roche, 5401127001), 26 Wüsch units/ml, 30μl of DNaseI (Roche, 4716728001), up to 3ml with diluted DMEM (300ml of DMEM, 4ml of Penstrep, up to 400ml with water)). After adding the same amount of diluted DMEM with 10% FBS, the remaining surrounding tissue was removed mechanically using fine forceps. Clean bone was washed with 0.8x PBS and transplanted into a wild type host from which the tibio-fibula was removed. For muscle transplantations, a small incision was made on the host calf skin using surgical scissors and a small piece of Venus$^+$ muscle was transplanted into the host calf region. For tendon transplantations, the Achilles tendon was isolated from a Venus$^+$ froglet and transplanted into the host calf region. For skin transplantation, half of the host calf/shank skin was replaced with Venus$^+$ donor skin. Bone was not injured by this procedure. The incision and replaced skin were closed using surgical sutures (B.Braun, G1111434). During operation, donor and host froglets were covered with clean paper towels wetted with MS-222 solution. The host animals were placed into sterile water with Pen/Strep after operation. 9-days after operation, the tissue grafted froglet was anesthetized in 0.03% MS-222 and their lower hind limb was amputated through the grafted site. 4-weeks after limb amputation, animals were anesthetized in 0.03% MS-222 and the regenerated spike was fixed in modified Zamboni fixative (2%PFA, 0.1% Saturated picric acid, 40mM NaH_2PO_4, 120mM Na_2HPO_4) overnight at 4°C, washed in PBS, treated with 8% EDTA/1xPBS pH7.4, incubated in 15% and 30% sucrose/1x PBS overnight at 4°C, and frozen in OCT compound (Science Service, 62550-12) and stored in -80°C ready for cryosection and further analysis.

Blastema collection and cell isolation

All tools were sterilized beforehand by autoclave. For cell transplantation experiments, 2.0 - 2.2 cm snout-to-cloaca stage 66 froglets and 8 - 9 cm snout-to-tail axolotls were used as the blastema donors. Regenerative blastema were prepared using stage 53 developing tadpoles. Green- (*CAGGs:Venus* for frogs; *CAGGs:GFP* for axolotls) or red- (*CMV:tdTomato* or *CAGGs:mCherry* for frogs; *CAGGs:mCherry* for axolotls) fluorescent animals of the correct stage and size were collected under a microscope. Legs of the selected frogs or axolotls were amputated with disposable scalpels at the upper leg level close to the knee. After the extruded bone was trimmed using spring scissors (Fine Scientific Tools, 15000-4), animals were allowed to recover in clean water briefly until bleeding stopped. They were then transferred to clean water with 0.5x Pen-Strep. Daily feeding and cleaning paradigms were applied until the blastema samples were ready to be collected and the animals were sacrificed after blastema collection.

On the day of blastema collection, blastema samples (blastema plus stump) were collected under a stereoscope (Olympus, SZX16) in a hood and washed twice in 0.7x PBS at room temperature. They were then dipped in 70% ethanol for 10 seconds and immediately washed twice in 0.7x PBS at room temperature. To expose the blastema mesenchyme, the muscle bundles surrounding the blastema were carefully removed by spring scissors under green or red fluorescence channel depending on the genotype of the animals. Blastema mesenchyme can be distinguished at the tip of the sample and was harvested using a disposable scalpel before being transferred to fresh 0.7x PBS. The blastema mesenchyme was chopped into <0.5mm cubes and immediately transferred to a tube of digesting solution (0.26WU/ml Liberase TM in 0.7x PBS). The enzymatic digestion was placed on a rotating wheel at room temperature for 45 minutes and then the cells were mechanically dissociated by pipetting 10-15 times with a P1000 pipet tip. Enzymatic reactions were stopped by adding 1x volume high-serum culture medium (HS-AMEM, 125ml MEM, 20ml heat inactivated FBS (Sigma-Aldrich, F7524), 2ml insulin (1mg/mL, Sigma-Aldrich, I5000), 2ml glutamine (200mM, Gibco, 25030-024), 2ml Pen/Strep (10000U/mL, Sigma-Aldrich, P0781), 50ml ddH_2O), and samples were filtered sequentially through 70 μm and 30 μm MACS SmartStrainers (Miltenyi Biotec, 130-098-458 and 130-098-462). Dissociated cells were then pelleted using 300x rcf centrifugation for 5 minutes at room temperature, then washed twice with 0.7x PBS before resuspension in serum-free medium (114.3ml F12:DM EM$^+$Glutmax (Gibco, 10565018), 1.5ml Sodium pyruvate (Gibco, 11360070), 1.5ml B27 supplement, 1.5ml MEM NEAA (Gibco, 11140050), 1.5ml insulin (1mg/mL, Sigma-Aldrich, I5000), 1.5ml Pen/Strep (10000U/mL, Sigma-Aldrich, P0781), 28.2ml ddH_2O) on ice. The concentration of cells was determined using a hemocytometer. For limb bud donor cells, stage 51 limb bud cells of fluorescent tadpoles were collected and prepared with the same procedure. For scRNA-seq library prep, dissociated frog cells were further filtered through a 10μm cell strainer (BD Biosciences, 340732).

Cell transplantation

The number of cells required for transplantation was calculated, and then pelleted in a sealed yellow Pipetteman tip by centrifugation. The yellow tip was then cut open near the level of cell pellet and placed on a transparent tape in a 3-cm petri-dish ready for loading. To load the injecting glass pipet with a high concentration of cells, the remaining medium in the yellow tip was first removed as much as possible without resuspending the pellet. The cells were then sucked directly into a glass pipet connected to a nanoject II system (Drummond SCI, 3-000-204). Meanwhile, stage 50 thymectomised wildtype tadpoles (Nieuwkoop and Faber, 1956) were anesthetized and laid belly-up on a piece of wet tissue paper in a 10-cm petri-dish. The limb bud was oriented under a stereoscope, the head and the tail regions were covered with additional pieces of wet tissue paper to prevent the animal from drying. The glass pipet pierced the epidermis at the proximal region of the limb bud and was moved distally until the tip of the pipet reached the distal mesenchyme without piercing the epidermis. Cells were then carefully injected into the distal region of the limb bud. Cells were injected into either one or both limb buds of the same tadpole. The transplantation procedure was repeated until the donor cells in the glass pipet were depleted. More than 10000 cells were estimated to be injected per limb bud (Figure S4K). The transplanted limb buds were

immediately imaged after transplantation (0-day post-transplantation, 0 dpt), and were traced two times per week until collection at around 4-5 weeks. Mature legs of frogs and axolotl were collected and fixed in 4% MEMFA (1x MEM (41.86g MOPS, 0.5g $MgSO_4$-$7H_2O$, 1.52g EGTA, dissolve in H_2O and fill up to 200mL, pH 7.4), 3.7% formaldehyde (Sigma-Aldrich, 1040031000)) on a rotor in a cold room overnight. Samples were washed three times in PBS before decalcification in 8% EDTA/PBS overnight in the cold room. The next day, the samples were washed three times in PBS and dehydrated with 30% sucrose overnight in the cold room. They were then embedded in OCT and stored in -20°C ready for cryosection and further analysis.

Cryosection, immunostaining and microscopy

Samples were sectioned into 8 μm thickness on loading slides with a cryostat (NX70, Thermo Scientific). Cryosections were dried and stored in -20°C. Before immunostaining, slides were thawed and were stained with primary antibodies against GFP (Rockland, 600-401-215, 1:1000, and MPI-CBG, Dresden, 1:1000), mCherry (Acris Antibodies, AB0040-200, 1:1000), Sox9 (Chemicon, Ab5535, 1:200, and R&D, AF3075, 1:200), Prrx1 (Gerber et al., 2018), Pax7 (MPI-CBG, Dresden, 1:200) and Col1A2 (Developmental Studies Hybridoma Bank, SP1.D8, 1:50). Alexa 488, Alexa 568, Alexa 647 (Invitrogen, 1:500, see key resources table for catalog details) were used as secondary antibodies. All sections were stained with DAPI (Sigma-Aldrich, D9542, 1:1000) and mounted in Mowiol 4-88/DABCO mounting medium (Sigma-Aldrich, 9002-89-5).

For samples of the bulk tissue transplantation, images were taken using an Olympus VS110 microscope and analyzed using FIJI and QuPath software (Bankhead et al., 2017). The number of Venus-labeled cells in the stump (500 micrometers from amputation plane) and Venus-labeled cells in the spike were counted. The number of Venus-labeled cells was calculated as a ratio of the percentages of Venus labeled cartilage cells in the spike over the total number of Venus labeled cells in the spike (Table S1). Two sections each from two different samples were used for counting. For the cell transplantation samples, images were taken with either a Zeiss Axio Imager Z2 (upright) with sCMOS camera, or a Zeiss LSM780 Axio Observer (inverted). At least 3 sections of each sample were counted using the ZEN Blue software.

Single-cell RNA sequencing

For frog blastema and limb bud samples of different stages, cells were isolated as mentioned above and cDNA generated following the Chromium Single Cell 3′ Kit protocol (10X Genomics, 3' library kit, v3 chemistry). For one of the mature uninjured and the 3 dpa samples, converted *Prrx1:CreER;CAGGs:lp-Cherry* cells from the upper legs were dissociated and isolated by FACS (FACSAria III, BD Biosciences) with a 100 μm nozzle prior to cDNA generation. Cell concentration was estimated manually using a hemocytometer and cells were diluted to obtain approximately 5,000-7,000 cells for non-pooled experiments and to obtain 12000-15000 cells in pooled experiments per lane of a 10x microfluidic chip device. Pooled experiments were performed for the blastema time course where cells of 3 different time points with each animal batch expressing a different fluorescent color signal were pooled and for the stage 54 limb bud cells that were pooled with a non-sorted mature uninjured tissue (0 dpa). Cells of blastema time points 7, 10 and 14 dpa (early blastema) were pooled and cells of blastema time points 14, 20 and 52 dpa (late blastema) were pooled, respectively. Single-cell cDNA and sequencing libraries were generated following the manufacturer recommendations (10X Genomics, 3' library kit, v3 chemistry). The quality of the cDNA and resulting sequencing libraries were checked by either bioanalyzer (High Sensitivity DNA Kit, Agilent, 5067-4626). The libraries were sequenced using Illumina NovaSeq platforms PE100 or PE150.

For axolotl limb bud samples, the stages of axolotl embryos were confirmed under a stereomicroscope before stage 50, 52, and 54 limb buds were collected. Cells of each stage, including epidermis, were dissociated and prepared using the same Liberase protocol described above. scRNA-seq libraries were prepared following the Chromium Single Cell 3' Kit protocol (10X Genomics, 3' library kit, v3 chemistry), and were sequenced using Illumina NovaSeq platforms PE100. For axolotl blastema samples, cells of two blastema time points (5 and 11 dpa) were isolated from *Prrx1:CreER* axolotl strains as described in (Gerber et al., 2018) without FACS enrichment. ScRNAseq experiments were performed following the Chromium Single Cell 3' Kit protocol (10X Genomics, 3' library kit, v2 chemistry) as described in Gerber et al. (2018). Three 10x lanes were used for 5 dpa blastema cells and two 10x lanes for 11 dpa cells. The quality of the cDNA and resulting sequencing libraries were checked by a bioanalyzer. The libraries were sequenced on an Illumina HiSeq2500.

Computational analysis

Cell Ranger (10x Genomics) was used to align sequencing reads using default parameters to the *Xenopus laevis* v9.2 reference genome with fluorescent marker genes being manually added to the reference. The genome was downloaded from Xenbase (http://www.xenbase.org/, RRID:SCR_003280) (Karimi et al., 2018). Reads originating from axolotl libraries were mapped against the latest axolotl genome release (Nowoshilow and Tanaka, 2020; Schloissnig et al., 2021) using STARsolo (STAR 2.7.5a) (Dobin et al., 2013) with parameters mimicking Cell Ranger's (10x Genomics) transcript counting strategy. Fluorescent marker genes were manually added to the references, respectively. Different versions of Seurat (Butler et al., 2018) were used throughout the analysis. Seurat v2 was used for raw data characterization and cell type assignment. Seurat v3.1 was used to generate all panels shown in the manuscript. Ribosomal protein genes and pseudogenes were excluded from the analysis besides the transplantation experiment analysis. Generally, cells with more than 60,000 or less than 1,000 detected transcripts, as well as those with a mitochondrial transcript proportion higher than 20% were excluded with some exceptions (see full information in Tables S2 and S3). When clusters were identified to be still driven only by low RNA counts in a first screening, cells belonging to these clusters were removed. For CT-enriched sorted cells some contaminating cell types such as epidermal cells were identified and removed after an initial screening using Seurat. *Xenopus laevis* carries a tetraploid genome

and encodes for almost all genes a L and S version of the same gene. Whenever L or S is not designated in the manuscript and both genes were expressed, the version with the higher expression intensity (most often L) is represented.

For visualizations in the main figures and the supplementary cell atlases, Seurat's built-in scale function was used to regress out differences in nUMI, nGene, percent.mt and cell cycle effects. Cell cycle effects were not considered in the first round of data screening. Scaling and PCA were always performed on all genes. Uniform Manifold Approximation and Projection (UMAP) was applied to the top principal components (PCs) for visualization. Data integration was performed for the blastema time course, the transplantation experiment, and combined limb bud and blastema data (frog and axolotl) using Seurat's built in Harmony (Korsunsky et al., 2019) function to reduce the confounding effect of different batches and samples. Running Harmony was always performed with default parameters and 50 input PCs. For the blastema time course the top 50 harmony components obtained were converted to positive values by adding the absolute minimum for each harmony component across the cells for that component. The corrected matrix was used as input into SPRING (Weinreb et al., 2018) using the SPRING webpage (https://kleintools.hms.harvard.edu/tools/spring.html). SPRING was run with 50 input PCs, 4 nearest neighbors and a gene variability percentile of 20% and no other filters were applied. The dynamic mode was used to visualize the SPRING embedding. The pseudotime estimate was calculated by a diffusion map analysis (Haghverdi et al., 2016) using the R package *destiny* (Angerer et al., 2016) followed by ranking cells based on their raw diffusion pseudotime. Gene ontology (GO) enrichment analyses were performed by using DAVID Bioinformatics Resources 6.7 (Huang et al., 2009) using time point specific cluster markers as input genes. Quadratic programming was performed using the R package *quadprog*. Top and bottom fold-change genes between mature and stage 54 limb bud samples based on time-point-averaged gene expression values were estimated by subtracting values of respective time points. Top and bottom 100 hits, respectively, were used as input gene set for quadratic programming. Fluorescent markers were removed when found on the list. Cartilage scores were obtained by summing expression values of shared cartilage marker genes for frog and axolotl blastema and limb bud developing cartilage cells. Common cartilage markers for frog developing cartilage were *col2a1.L*, *col2a1.S*, *col9a1.L*, *col11a2p1.S*, *col9a2.S*, *col9a3.L*, *col9a2.L*, *LOC108702653*, *matn4.L*, *matn4.S*, *col9a1-b*, *otos.S*, *otos.L*, *LOC101730276.L*, *fgfr3.L*, *spock3.S*, *rspo3.L*, *fgfrl1.S*, *plod2.L*, *fth1.L.1*, *LOC108717350*. Common cartilage markers for axolotl developing cartilage were matn1, acan, crip1, hapln1, otos, cnmd, fgfbp2, epyc, c17orf67, loc108704014, col11a2, col9a3, col2a1, papss2, col9a1, ecrg4, loc115080956, col9a2, pdcd6, col11a1, rbp4, ucma, clec3a, matn4, fbln7, papss1, cthrc1, nog, loxl3, plod2, hapln3, pcolce, xylt1, fgfr3, sox9, tgm2, loc115477099, sox6, pdgfrl, cox4i2, scrg1, gyg1, sox8, smoc1, aldob, cpa6, lmcd1, chst3, sfrpx, loc104277804, loxl4, ldhb, slc35d1, mob2, srpx. Differentially expressed genes between frog or axolotl limb bud and blastema cartilage development were identified by using Seurat's default DE analysis function, respectively, by comparing cells having a high cartilage score in either frog limb buds or blastema against cells that have a lower score in the same sample type as well as all cells of the other tissue type and vice versa.

In addition, a recently published scRNA-seq data set (GEO accession number: GSM3206455) on axolotl blastema formation was re-analyzed (Samples: GSM3206452, GSM3206453, GSM3206454, GSM3206455, GSM3206456, GSM3206457, GSM3206458, GSM3206459) (Gerber et al., 2018).

Identifying samples in pooled scRNA-seq

For pooled *Xenopus* scRNA-seq experiments samples were identified by expression of fluorescent markers in an initial screening using Seurat and doublet discrimination was performed based on fluorescent label expression. However, some fluorescent markers were weakly expressed and showed therefore a poor detection rate, hampering sample and doublet assignment. For the blastema time course, cells of the 10 dpa sample (early blastema pool) and the 20 dpa sample (late blastema pool) had almost no fluorescent signal detected. As the separation of early and late blastema was possible through the different batches we assigned all cells without a detected fluorescent label to 10 dpa for the early blastema and to 20 dpa for the late blastema. Potential doublets and misassigned blastema time points that were potentially not identified due to missing fluorescent signal do not critically interfere with the conclusions we state in the manuscript. Similarly, the fluorescent label for the mature cells in the stage 54 limb bud–mature pooled experiment was affected. In contrast to the blastema pool, cells could be easily differentiated by their expression profile and mature CT cells could be isolated from stage 54 limb bud cells by selecting cells from sample specific clusters.

After isolating individual samples from pooled experiments, cells that passed quality control were clustered as mentioned above. The CT cell clusters of each sample (pooled and non-pooled experiments) were identified by CT-specific markers (e.g. *prrx1*) and then isolated using the subset function in Seurat. The extracted CT cells of respective time points were computationally pooled prior to proceeding to time course analyses shown in Figures 2 and 3A.

QUANTIFICATION AND STATISTICAL ANALYSIS

At least three independent experiments were performed for each quantification unless specified. All quantifications were performed with at least three animals, with a minimal of three representative and distinct sections being imaged and counted per animal. Two-tailed unpaired Student's t test was performed using GraphPad Prism version 8 and 9 for macOS (GraphPad Software, San Diego, California USA, www.graphpad.com). Data were presented as mean ± standard deviation (SD). Asterisks indicate statistically significant difference between groups. n.s., not significant; *, $P < 0.05$; **, $P < 0.01$; and ***, $P < 0.001$. The statistical details can also be found in the corresponding figure legends.